Total solar eclipse over Antarctica on 23 November 2003 and its effects on the atmosphere and snow near the ice sheet surface at Dome Fuji

Takao Kameda,[1] Koji Fujita,[2] Okimasa Sugita,[3] Naohiko Hirasawa,[4] and Shuhei Takahashi[1]

[1] The Moon cast a long shadow over Antarctica on 23 November 2003 in a total solar eclipse. The eclipse was observed at Dome Fuji Station, located at the highest point of East Dronning Maud Land, Antarctica, and lasted 1 h 41 min 37 s in a cloudless condition, during which the Sun was completely obscured for 1 min 43 s. This was the first total solar eclipse to be observed in the Antarctic ice sheet. During the eclipse at Dome Fuji, the air temperature at 1.5 m above the snow surface and the subsurface snow temperature decreased by 3.0 K and 1.8 K, respectively. Estimated surface snow temperatures decreased by 4.6 K. Atmospheric pressure and wind direction did not change, but the wind speed possibly decreased by 0.3 m/s with decreasing air temperature; natural variations in wind speed before and after the eclipse made it difficult to identify a true effect of the solar eclipse. Variations of energy components (net shortwave and longwave radiations, sensible and latent heat fluxes, and geothermal heat) during the eclipse were investigated. The total loss of global solar radiation during the eclipse was 0.60 MJ m^{-2}, equaling 1.6% of the total daily global solar radiation. Regional effects of the eclipse due to a reduction of global solar radiation for air temperature and snow temperature ranged from 0.015 to 0.020 K (W m^{-2})$^{-1}$. We additionally examined the relation between eclipse obscuration (the fraction of the Sun's surface area occulted by the Moon) and the reduction of global solar radiation from the first to second contacts. The eclipse was also observed from space by the Moderate Resolution Imaging Spectroradiometer (MODIS) sensors onboard NASA's Terra and Aqua satellites. The observational results of this study will contribute to detailed model calculations for clarifying the meteorological effects of eclipses.

1. Introduction

[2] The Moon created a total solar eclipse over Antarctica on 23 November 2003. The eclipse was observed at Dome Fuji Station (77°19′01″S, 39°42′11″E; 3810 m a.s.l; annual mean air temperature −54.4°C), located at the highest point of East Dronning Maud Land, Antarctic ice sheet. The eclipse lasted 1 h 41 min 37 s in a cloudless condition, during which the Sun was completely obscured for about 1 min 43 s. This was the first total solar eclipse to be observed in the Antarctic ice sheet. Since Captain James Cook first

sailed around Antarctica in the 1770s, 18 total solar eclipses have occurred over Antarctica [*Espenak and Meeus*, 2006]; however, probably no one observed the total solar eclipse in Antarctica (see Appendix A for details). Eight members of the 44th Japanese Antarctic Research Expedition (JARE-44), engaged in glaciology, meteorology, and upper atmosphere physics research as well as preparations for ice coring at Dome Fuji Station [*Kameda et al.*, 2005, 2007], observed the 23 November 2003 eclipse.

[3] A number of reports since the nineteenth century have described the meteorological effects of solar eclipses [e.g., *Upton and Rotch*, 1893; *Clayton*, 1901; *Kimball and Fergusson*, 1919; *Ueshima et al.*, 1949; *Anderson et al.*, 1972; *Stewart and Rouse*, 1974; *Anderson and Keefer*, 1975; *Fernández et al.*, 1996; *Segal et al.*, 1996; *Eaton et al.*, 1997; *Anderson*, 1999; *Hanna*, 2000; *Leeds-Harrison et al.*, 2000; *Ahrens et al.*, 2001; *Foken et al.*, 2001; *Szalowski*, 2002; *Aplin and Harrison*, 2003; *Garasopoulos et al.*, 2007] (see also K. C. Crawford et al., The annular eclipse of 10 May 1994: Atmospheric responses observed by the Oklahoma mesonetwork, paper presented at 9th AMS Con-

[1]Snow and Ice Research Laboratory, Kitami Institute of Technology, Kitami, Japan.
[2]Graduate School of Environmental Studies, Nagoya University, Nagoya, Japan.
[3]Observations Department, Japan Meteorological Agency, Tokyo, Japan.
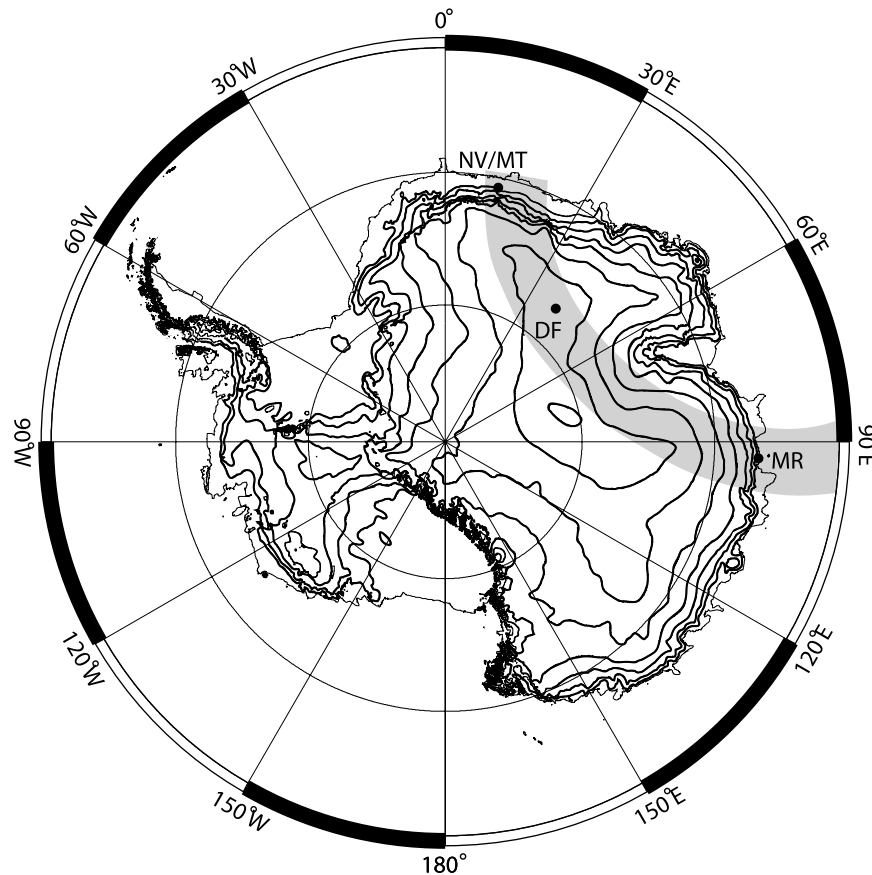[4]National Institute of Polar Research, Tokyo, Japan.

Figure 1. Locations of Dome Fuji Station (DF) and the total eclipse band. The other three stations in the band, all along the coast, are also shown (MR, Mirny; NV, Novolazarevskaya; and MT, Maitri; the first two stations are Russian, and the third is Indian).

ference on Applied Climatology, American Meteorological Society, Boston, Massachusetts, 1995). Eclipses are spectacular events that occur infrequently and provide a unique opportunity to investigate the atmosphere's reaction to sudden changes in solar radiation. However, eclipses have often been observed under cloudy conditions, making it difficult to properly estimate their effects on the atmosphere.

[4] Recent studies have extensively investigated the meteorological effects of solar eclipses using model calculations [e.g., *Gross and Hense*, 1999; *Prenosil*, 2000; *Vogel et al.*, 2001; *Founda et al.*, 2007; *Eckermann et al.*, 2007]. In particular, *Eckermann et al.* [2007] used a global numerical weather prediction model to clarify the regional (East Africa to Australia) and altitudinal (from the surface to 90 km in altitude) effects of the total solar eclipse of 4 December 2002. They reported that surface air temperature decreased by ~4 K at maximum in South Africa and surface atmospheric pressure oscillated at 0.1–0.5 hPa after the eclipse in a broad area along the eclipse's band; these findings are broadly consistent with surface atmospheric observations of some previous studies (see, e.g., *Segal et al.* [1996] for air temperature decrease and *Anderson et al.* [1972] for atmospheric pressure oscillations).

[5] Here, we report on the total solar eclipse of 23 November 2003, as observed from space and from the ice sheet surface at Dome Fuji. We describe the meteorological effects on the atmosphere and snow, and also changes in radiation and heat transfer near the ice sheet surface during

the eclipse at Dome Fuji. Although *Vats et al.* [2006] described shadow bands during the total solar eclipse of 23 November 2003 near Maitri Station, and *Rashid et al.* [2006] described the ionospheric response to the eclipse, the effect of the eclipse on the atmosphere and snow near the surface of the ice sheet was not reported. We also summarize previously reported findings on the meteorological effects of eclipses on the atmosphere near the ground.

2. Observation Site and Methods on the Ice Sheet

[6] Figure 1 shows the area of total solar eclipse on 23 November 2003 (redrawn from *Espenak and Anderson* [2002]) and the location of Dome Fuji Station (DF). Dome Fuji Station was located close to the center of the eclipse band and on a nearly flat snow surface. *Esaki et al.* [2007] described the meteorological observation system at Dome Fuji Station in 2003, and *Hirasawa and Fujita* [2008] described the methodology and results of solar (shortwave) and infrared (longwave) radiation observations in 2003. However, because these papers were written in Japanese, we describe the observational method again.

[7] Global solar radiation ($R_{S\downarrow}$: downward shortwave) and reflected shortwave radiation ($R_{S\uparrow}$) were measured using two pyranometers (Model MS-801F for downward, Model MS-801 for upward; EKO Instruments Trading Co., Ltd., Japan; time constant of 2.5 s). Both sensor plates were located 2.2 m above the snow surface. The measured range
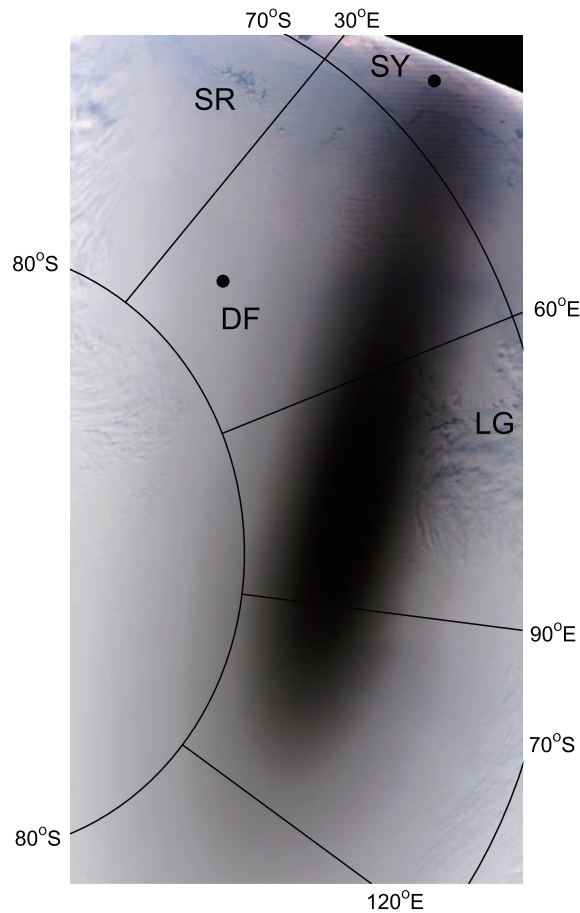
Figure 2. Lunar shadow over Antarctica captured by MODIS on the Terra satellite from 2253 to 2301 UTC on 23 November. DF, Dome Fuji Station; SY, Syowa Station; SR, Sør-Rondane Mountains; and LG, Lambert Glacier. The image is expressed using Lambert azimuthal equal-area projection and is provided by the NASA/GSFC/MODIS Rapid Response Team.

the glass dome under cold conditions. Data were measured at 6-s intervals and automatically averaged over 1-min periods by the measurement instruments, resulting in one datum per minute for each measured quantity (e.g., the value for 0001:00 was obtained from the ten measurements between 0000:06 and 0001:00). The pyranometers and pyrgeometers had ±1.5% accuracy.

[9] Air temperature was measured at 3-s intervals using a Pt 100 sensor (Model E-734, Yokogawa Denshikiki Co., Ltd., Japan; diameter 6 mm, length 122 mm; time constant for air of 68 s) in a ventilated shelter (Model E-834, Yokogawa Denshikiki Co., Ltd., Japan; ventilation speed: 5−7 m/s) at 1.5 m height above the snow surface.

[10] Snow temperature at 0.05 m depth was measured at 1-min intervals using a Pt 100 sensor, and snow temperatures at other depths (0.19, 0.24, 0.29, 0.39, 0.59, 0.99, 1.13, 1.62, 2.12, 3.12, 6.12, and 11.12 m) were measured at 10-min intervals using Pt 100 sensors. Sensors of air and snow temperatures had an accuracy of 0.1°C.

[11] Atmospheric pressure was measured at 3-s intervals in a room (W 8.1 m × L 4.5 m × H 2.5 m) located 2.7 m beneath the snow surface using a pressure sensor (Model F4711, Yokogawa Denshikiki Co., Ltd., Japan). The accuracy of the atmospheric pressure was ±0.15 hPa. Wind speed and direction at 10 m height were measured at 3-s intervals using an aerovane (Model 05103, R. M. Young Co., USA). The accuracies of wind speed and direction were ±0.3 m/s and ±3°, respectively. The 1-min average data for air temperature, snow temperature at 0.05 m depth, atmospheric pressure, wind speed, and wind direction were calculated using the 3-s interval data (e.g., the value for 0001:00 was obtained from the 20 measurements between 0000:03 and 0001:00).

[12] Two types of data logger (Model C-CR10X-2M, Campbell Scientific Inc., USA; Model KADEC-US6, Kona System Co., Ltd., Japan) and personal computers were used for data collection. Digital video and cameras were used for recording the nature of the eclipse.

3. Results

3.1. Observational Results From Space

[13] Figure 2 shows a satellite image of the eclipse over Antarctica by the Moderate Resolution Imaging Spectroradiometer (MODIS) on the Terra satellite launched by NASA on 18 December 1999. The original image was acquired by the satellite line by line from approximately 2253 to 2301 UTC, and projected to Lambert Azimuthal equal-area projection by NASA Goddard Space Flight center (GSFC)/MODIS Rapid Response Team. The time interval is close to the instant of greatest eclipse at 2249:17 UTC in Wilkes Land (72°40′00″S, 88°22′36″E [*Espenak and Anderson*, 2002]). The Moon's shadow has two parts: the fuzzy outer shadow called the penumbra and the dark inner shadow called the umbra (approximately 480 km for the major axis and 140 km for the minor axis [*Espenak and Anderson*, 2002]). Within the umbra, the Sun is completely blocked by the Moon, creating the total solar eclipse seen by ground observers. Since the solar angle was approximately 17°, the Moon cast a long shadow over Antarctica. Clouds were observed at the left side of the image.

of shortwave radiation was 0.305−2.8 μm. *Hirasawa and Fujita* [2008] reported that the reflected shortwave radiation ($R_{S\uparrow}$) contained some systematic errors due to frost. Thus, instead of $R_{S\uparrow}$, we estimated $R_{S\uparrow}$ using data for $R_{S\downarrow}$ and albedo at the surface snow. We selected an albedo value of 0.85 based on findings by *Yamanouchi* [1983], who investigated the albedo of a similar surface snow condition (new snow particles on the snow surface under a clear-sky condition with solar elevation angle of 10°) at Mizuho Station, East Antarctica, from 6 to 14 November 1979.

[8] Downward longwave radiation ($R_{L\downarrow}$) and upward longwave radiation ($R_{L\uparrow}$) were measured using two pyrgeometers (both MS-200F; time constant of 15 s). Both sensor plates were located at 1.9 m height using the same tower that held the two pyranometers. The measured range of longwave radiation was 3−50 μm. The pyrgeometers employed a thermistor-resistance circuit to correct for heating by global solar radiation, as discussed by *Albrecht et al.* [1974] and *Hirasawa and Fujita* [2008]. For the "F" model of pyranometer and pyrgeometers, a 75-mm-diameter fan was enclosed at the bottom of the sensor to avoid frost on

Figure 3. Total solar eclipse at Dome Fuji Station.

[14] During the eclipse, the umbra and the penumbra moved from east (Mirny Station area in Figure 1) to the west (around Novolazarevskaya and Maitri Stations in Figure 1) at an average speed of about 5000 km/h (~1400 m/s [*Espenak and Anderson*, 2002]) over Antarctica. Therefore, Figure 1 illustrates the geographical trace of the umbra during the eclipse. A companion satellite, Aqua, also captured an image of the eclipse between 2315 and 2320 UTC, when the Moon's shadow covered the area of 0°–20°E, 70°S–82°S over Antarctica. The image is shown as an "Image of the Day" in "Earth Observatory" on a website operated by the NASA/GSFC/MODIS Rapid Response Team (http://earthobservatory.nasa.gov/IOTD/view.php?id = 3994).

3.2. Observational Results at Dome Fuji

3.2.1. General Description of the Eclipse

[15] We observed the solar eclipse in a completely cloudless condition at Dome Fuji. The Moon first made contact with the Sun from the left at 2217:47 UTC on 23 November (local time (LT) was 0117:47 on 24 November; hereafter, local time is used for better understanding of the "real time" at Dome Fuji). The vertical angle of the Sun was 8.3° from the horizon. Total solar eclipse started at 0207:33 LT (i.e., "second contact") when the vertical angle of the Sun was 9.3°. Figure 3 shows the condition during the total solar eclipse; some buildings and construction machinery are visible at the lower left. The total eclipse ended at 0209:16 LT ("third contact") at a vertical angle of 9.4°. A "diamond ring" was observed. During the eclipse, Venus, Mercury, and some bright stars were clearly visible, and the

sky brightened from the horizon to approximately 5° in vertical angle, almost completely surrounding us. However, this light was not observed directly below the Sun at approximately 20° in horizontal angle (10° on either side of the Sun), which was the area of the shadow of the Moon (umbra). Figure 3 shows part of the light and the shadow. The solar eclipse ended at 0259:24 LT ("fourth contact") when the vertical angle of the Sun was 10.9°. The major and minor axes of the umbra at Dome Fuji were approximately 770 km and 110 km, respectively [*Espenak and Anderson*, 2002].

[16] Using the computer program "EclipseNavigator" (AstroArts, Inc. Japan), the contact times of the eclipse and the vertical angles of the Sun were calculated for the position of Dome Fuji using Besselian elements for the total solar eclipse of 23 November 2003 provided by NASA (http://eclipse.gsfc.nasa.gov/SEbeselm/SEbeselm2001/SE2003Nov23Tbeselm.html). The calculations were made for the mean limb (center of mass) of the Moon, thus the contact times have been rounded to the nearest second. The corrections of the second and third contact times for the true lunar limb profile described by *Espenak and Anderson* [2002] were +0.2 s and −3.0 s, respectively; thus the third contact at Dome Fuji was possibly 0209:13 LT.

3.2.2. Meteorological Conditions

[17] Global solar radiation ($R_{S\downarrow}$; Figure 4a) gradually decreased from 0120 LT (average of ten measurements taken between 0119:06 and 0120:00 LT), approximately 2 min after the start of the eclipse, and reached zero during the total solar eclipse. Downward longwave radiation ($R_{L\downarrow}$;
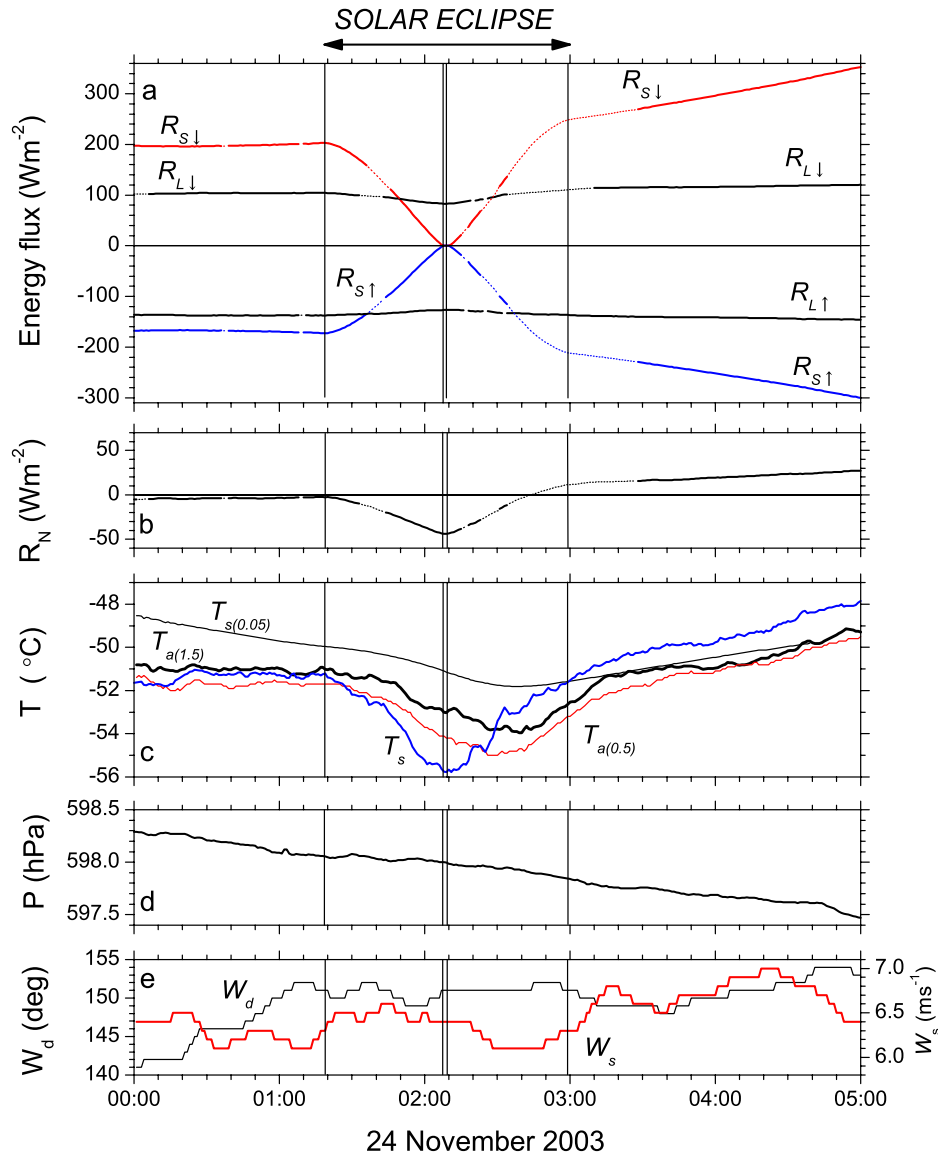
Figure 4. (a) Global solar radiation ($R_{S\downarrow}$), reflected shortwave radiation ($R_{S\uparrow}$) calculated from $R_{S\downarrow}$ and albedo (0.85), downward and upward longwave radiation ($R_{L\downarrow}$ and $R_{L\uparrow}$). (b) Net radiation calculated from the four radiation components ($R_N = R_{S\downarrow} + R_{S\uparrow} + R_{L\downarrow} + R_{L\uparrow}$). (c) Air temperature ($T_{a(1.5)}$ and $T_{a(0.5)}$) measured at 1.5 m and 0.5 m above the snow surface, snow-surface temperature (T_s) calculated from upward longwave radiation with the Stefan-Boltzmann constant, and snow temperature ($T_{s(0.05)}$) measured at 0.05 m depth. (d) Atmospheric pressure measured in a room located 2.7 m beneath the snow surface. (e) Wind speed (W_s) and wind direction (W_d) measured at 10 m above the snow surface. The first, second, third, and fourth contacts are indicated by vertical lines. Missing data, which were estimated by smooth interpolation, are indicated by dotted lines. Local time at Dome Fuji is used (LT = UTC + 3 h).

Figure 4a) and upward longwave radiation ($R_{L\uparrow}$; Figure 4a) changed slightly during the eclipse. Before the eclipse, net radiation (R_N; Figure 4b) was slightly negative and began to decrease from 0140 to 0232 LT, during which time the snow surface was radiatively cooled. The air temperature at 1.5 m height ($T_{a(1.5)}$; Figure 4c) gradually decreased from approximately 0122 LT, about 4 min after the start of the eclipse. The rate of decrease accelerated from 0147 LT when the Sun was 49.6% obscured by the Moon. (Eclipse obscuration, E_O, the fraction of the Sun's surface area occulted by the Moon, was 0.496. Eclipse magnitude, E_M, the fraction of the Sun's diameter occulted by the Moon, was 0.588.) The minimum

$T_{a(1.5)}$ was $-54.0°C$ at 0239 LT, a delay of about 30 min from the third contact. $T_{a(1.5)}$ gradually increased from 0249 LT. Since the air temperature at 0122 LT was $-51.0°C$, the maximum temperature decrease was 3.0 K. $T_{a(1.5)}$ returned to the noneclipse temperature level at approximately 0315 LT. The air temperature at 0.5 m height ($T_{a(0.5)}$; Figure 4c) decreased from $-51.8°C$ at 0128 LT and reached a minimum of $-55.0°C$ at 0229 LT, about 20 min after the third contact. The maximum decrease was 3.2 K. $T_{a(0.5)}$ returned to the noneclipse temperature level at approximately 0309 LT.

[18] The snow temperature at 0.05 m depth ("subsurface snow temperature," $T_{s(0.05)}$; Figure 4c) gradually decreased before the eclipse; the rate of decrease then accelerated from approximately 0130 LT, probably owing to the eclipse. The value of $T_{s(0.05)}$ reached a minimum at 0239 LT, which was the same timing as the air temperature minimum at 1.5 m height. The maximum decrease was 1.8 K. $T_{s(0.05)}$ returned to the noneclipse temperature level at approximately 0430 LT. After 0439 LT, $T_{s(0.05)}$ data were affected by an artificial shadow at the measuring point and are thus not shown.

[19] The surface snow temperature (T_s; Figure 4c) was calculated from upward longwave radiation ($R_{L\uparrow}$) under the blackbody assumption; that is, the emissivity of the surface snow was assumed to be 1.0, a value commonly used in previous studies involving surface energy balance calculations on the Antarctic snow [e.g., *King and Connolley*, 1997; *Reijmer and Oerlemans*, 2002; *van As et al.*, 2005]:

$$T_s = \left(\frac{|R_{L\uparrow}|}{\sigma} \right)^{\frac{1}{4}}, \tag{1}$$

where σ is the Stefan-Boltzmann constant (5.67×10^{-8} W m^{-2} K^{-4}). The value of T_s decreased from 0117 LT and reached its minimum of $-55.8°$C at 0208 LT. The maximum temperature decrease was 4.6 K, and T_s returned to its noneclipse level at approximately 0259 LT.

[20] Atmospheric pressure (Figure 4d) gradually decreased during the solar eclipse because of ordinary weather variation. Although some small oscillations in atmospheric pressure were identified, the oscillations also occurred before the eclipse. Thus, we consider the eclipse to have had no apparent effect on atmospheric pressure within the analytical resolution. For wind speed (W_s; Figure 4e), a small increase of 0.4 m/s was observed from 0112 to 0124 LT. The increase began 7 min before first contact and ended 5 min after first contact. A small decrease of 0.3 m/s was also observed from 0220 to 0248 LT, between the third and fourth contacts. There was no clear influence of the eclipse on wind direction (W_d; Figure 4e).

4. Discussion of Observational Results at Dome Fuji

4.1. Effect of Sensor Inertia

[21] When measuring rapidly changing phenomena, it is important to consider the inertia of sensors (or the "dynamic performance" of sensors). According to *Brock and Richardson* [2001] and *Foken* [2008], dynamic error (ε_d), which is the difference between the "true value" and the "measured value affected by the inertia of the sensor under a constant decreasing condition," is estimated as follows:

$$\varepsilon_d = -a\tau(1 - e^{-t/\tau}), \tag{2}$$

where a is the average decreasing rate of the value, t is the time from the start of the decrease, and τ is a time constant of the sensor. Since rapid changes in global solar radiation and temperatures were observed during the eclipse, we will consider the effect for these parameters.

[22] The time constant of the pyranometer and the average decreasing rate of $R_{S\downarrow}$ from 0119 to 0208 LT were 2.5 s and -6.9×10^{-2} W m^{-2} s^{-1}, respectively. According to

equation (2), dynamic error of $R_{S\downarrow}$ during the time interval was 0.17 W m^{-2}. This value is smaller than the analytical errors of the sensors (± 3 W m^{-2}; $\pm 1.5\%$ accuracy for the maximum value of $R_{S\downarrow}$, 203 W m^{-2}, from 0119 to 0208 LT). Thus, we need not consider the inertia of the pyranometer for $R_{S\downarrow}$. Since a smaller rate of change was observed for $R_{S\uparrow}$ than for $R_{S\downarrow}$, and the time constant of the sensor for $R_{S\uparrow}$ is the same as that for $R_{S\downarrow}$, we also need not consider the effect on $R_{S\uparrow}$.

[23] The time constant of the thermometer for $T_{a(1.5)}$ and the average decreasing rate of $T_{a(1.5)}$ from 0122 to 0239 LT were 68 s and -6.5×10^{-4} K s^{-1}, respectively. We found that the dynamic error for $T_{a(1.5)}$ gradually decreased from 0.026 to 0.044 K from 0123 to 0128 LT, and the value became nearly constant at 0.044 K from 0128 to 0239 LT. Thus, the relatively large time constant of the thermometer (68 s) does not essentially affect $T_{a(1.5)}$ if we use the data at a resolution of 0.1 K.

[24] The average decreasing rate of $T_{a(0.5)}$ from 0128 to 0229 LT was -8.7×10^{-4} K s^{-1}. We found that the dynamic error for $T_{a(0.5)}$ gradually decreased from 0.034 to 0.059 K from 0123 to 0128 LT and became nearly constant at 0.059 K from 0128 to 0239 LT. This means that true $T_{a(0.5)}$ was 0.1 K lower than measured $T_{a(0.5)}$ from 0128 to 0239 LT if we express $T_{a(0.5)}$ at a resolution of 0.1 K. Thus, we concluded that the maximum air temperature decrease of $T_{a(0.5)}$ at 2:29 was 3.3 K, which is 0.1 K larger owing to the thermal inertia of the sensor.

[25] Snow density data at Dome Fuji from the surface to 1.0 m (0.29 to 0.34 g/cm^3 [*Takahashi and Kameda*, 2007]) and thermal conductivity data for Antarctic snow (Log $k = 2.6\rho - 3.0$, units of k and ρ are W m^{-2} s^{-1} and g/cm^3, respectively [*Lange*, 1984]) suggest that thermal conductivity (k) of snow from the surface to 1.0 m depth ranges from 0.1 to 0.3 W m^{-2} s^{-1}. Thermal conductivity of snow at Dome Fuji is about 100 times larger than that of the atmosphere (2.0×10^{-2} W m^{-2} s^{-1} [*National Astronomical Observatory*, 2008]). Thus, the effect of thermal inertia of the sensors in the snow is negligible.

4.2. Vertical Profiles of Air and Snow Temperatures From 0000 to 0500 LT on 24 November

[26] Figure 5 shows vertical profiles of air and snow temperature before, during, and after the eclipse. The air temperature profile was stable before the eclipse from 0000 to 0100 LT. When the eclipse started, the surface snow was cooled by the reduced radiative net balance (R_N) and reached a minimum at 0209 LT as described in section 3.2. At 0220 LT, the surface snow temperature increased; however, the air temperature continued to decrease because of the thermal inertia of the atmosphere. Sensible heat flux from and to the atmosphere (H_s) and energy flux from and to the deeper snow layer to the surface (H_G) will be briefly discussed in section 4.3.

4.3. Energy Budget at the Snow Surface From 0000 to 0500 LT on 24 November

[27] We examined the energy budget at the snow surface before, during, and after the solar eclipse. The snow surface was assumed to be sufficiently smooth to produce homogenous radiation; this assumption for the snow surface is reasonable, as shown by *Kameda et al.* [2008, Figures 5a
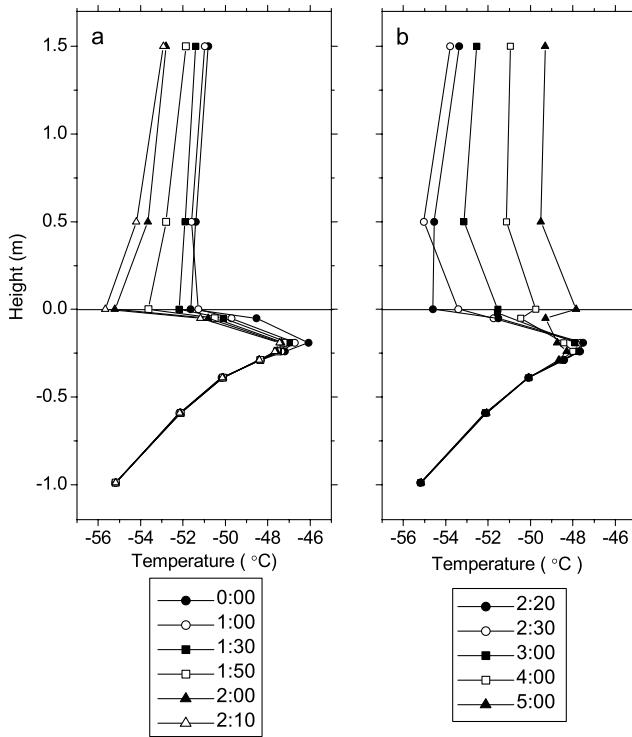
Figure 5. Vertical profile of temperature from 1.5 m above the snow surface to 0.99 m depth in the snow before and after the total solar eclipse, shown by local time at Dome Fuji (LT = UTC + 3 h). (a) From 0000 to 0210 LT. (b) From 0220 to 0500 LT.

and 5b] for surface snow conditions at Dome Fuji in 2003. Thus, only vertical fluxes needed to be considered. The principal components of the energy budget at the surface are

$$R_{Ns} + R_{NL} + H_s + H_L + H_G = 0, \tag{3}$$

where R_{Ns} is net shortwave radiation, R_{NL} is net longwave radiation, H_s is sensible heat flux from and to the atmosphere, H_L is latent heat flux from and to the atmosphere, and H_G is energy flux from and to the deeper snow layer. Here, we use sign conservation so that all of the radiative and nonradiative fluxes directed to the surface are positive and all those directed away from the surface are negative. Figure 6 shows these components.

[28] Net shortwave radiation R_{Ns} was estimated as described in section 2 and as follows:

$$R_{Ns} = R_{S\downarrow} + R_{S\uparrow} = (1 - 0.85)R_{S\downarrow}. \tag{4}$$

Net longwave radiation R_{NL} was assumed to be only absorbed at the snow surface. Thus, R_{NL} was calculated as

$$R_{NL} = R_{L\downarrow} + R_{L\uparrow}. \tag{5}$$

[29] Sensible heat flux (H_s) was calculated using the bulk transfer method [e.g., *Arya*, 2001], which is based on bulk transfer formulas,

$$H_S = c_p\,\rho\,C_H\,U_{1.0}(T_{a(1.0)} - T_s), \tag{6}$$

where c_p, ρ, and C_H are the specific heat (1.03×10^3 J kg^{-1} K^{-1} [*Touloukian and Makita*, 1970]) for average air temperature and atmospheric pressure conditions during the eclipse ($-52.6°$C and 593.0 hPa), the density of air (0.946 kg m^{-3} [*National Astronomical Observatory*, 2008]) for the same condition, and a bulk transfer coefficient (2.0×10^{-3} [*Kondo and Yamazawa*, 1986]), respectively. $U_{1.0}$ and $T_{a(1.0)}$ are wind speed and air temperature at 1.0 m height, respectively, and $U_{1.0}$ was derived from wind speed data at 10 m (W_s; Figure 4e) using the following equation:

$$U_{1.0} = W_s \ln(1.0/z_0)/\ln(10/z_0), \tag{7}$$

in which the roughness parameter z_0 equals 0.0002 m [*Royal Aeronautical Society*, 1972; *Kondo*, 2000; *Arya*, 2001]. $T_{a(1.0)}$ was calculated from the average of air temperatures at 0.5 and 1.5 m heights.

[30] Heat flux (H_G) from the surface to subsurface snow was calculated as

$$H_G = k(T_{s(0.05)} - T_s)/0.05, \tag{8}$$

in which k is the thermal conductivity of snow (0.3432 W m^{-1} K^{-1} for snow density of 300 kg m^{-3} at $-60°$C [*Weller and Schwerdtfeger*, 1977]). We measured the surface snow density from the surface to 0.03 m depth using a constant volume sampler (99.0 cm^3) on 14 November 2003; the resulting density was 299 kg m^{-3} [*Kameda et al.*, 2007].
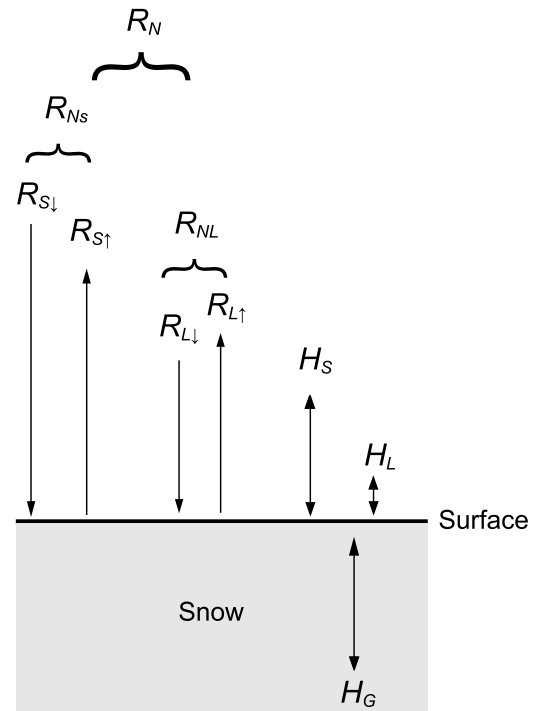

Figure 6. Main components of radiation and heat at the snow surface: net shortwave radiation (R_{Ns}), net longwave radiation (R_{NL}), global solar radiation ($R_{S\downarrow}$), reflected shortwave radiation ($R_{S\uparrow}$), downward and upward longwave radiations ($R_{L\downarrow}$ and $R_{L\uparrow}$), sensible heat (H_S), latent heat (H_L), and geothermal heat (H_G).
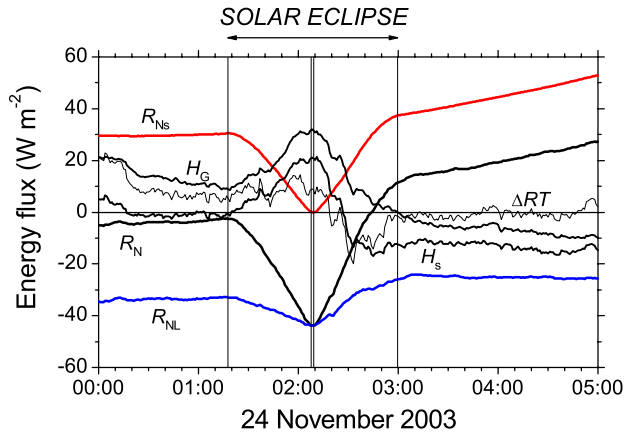
Figure 7. Radiation and heat components before and after the total solar eclipse: net shortwave radiation (R_{Ns}), net longwave radiation (R_{NL}), sensible heat (H_S), geothermal heat (H_G), and the residual term (ΔRT). The average latent heat (H_L) from 0000 to 0500 LT was small (≈ -0.4 W m^{-2}) and is therefore not shown. Local time at Dome Fuji is used (LT = UTC + 3 h).

[31] Latent heat flux (H_L) caused by sublimation at the snow surface was calculated by two sublimation snow pans located at the snow surface at Dome Fuji. *Kameda et al.* [1997] used and reported on a similar method; the pans were glass "Petri dishes" (diameters: 9.65 cm and 9.05 cm, depths: 2.0 cm) filled with surface snow. The weights of the two snow pans were measured at 1720 LT on 23 November and at 0900 LT on 24 November. We found that the two snow pans had lost 0.05 g of weight, caused by sublimation at the snow surface. If we assume that the sublimation rate was constant during the time interval, these measurements allow us to estimate the average loss of surface snow by sublimation from 0000 to 0500 LT. The rate (ΔM) was -1.2×10^{-7} kg m^{-2} s^{-1}. Latent heat flux was estimated using the above rate and also the latent heat of ice sublimation (L_s) at $-50°$C (2.838×10^6 J kg^{-1} [*Mellor*, 1977],

$$H_L = \Delta M \, L_s = -1.2 \times 10^{-7} \times 2.838 \times 10^6 \approx -0.4, \quad (9)$$

where the unit of H_L is W m^{-2}.

[32] Figure 7 shows the changes in these components and a residual term (ΔRT) from 0000 to 0500 LT on 24 November. Since the value of H_L was small, H_L is not shown in Figure 6. The residual term (ΔRT) is defined as follows:

$$\Delta RT = R_{Ns} + R_{NL} + Hs + H_L + H_G. \quad (10)$$

We calculated the average ΔRT at 1-min intervals from 0000 to 0500 LT by the following equation:

$$\overline{\Delta RT} = \frac{\sum \left(\sqrt{(\Delta RT)^2} \right)}{300}. \quad (11)$$

The value of $\overline{\Delta RT}$ was 6.0 W m^{-2}, and the maximum and minimum ΔRT ranged from $+22.8$ to -19.9 W m^{-2}, respectively.

[33] The reason for the relatively large ΔRT from 0000 to 0300 LT is not known, but we speculate that estimation of H_S and H_G may contribute to the error. So, we briefly describe the variations of each energy component. Before the eclipse from 0000 to 0119 LT, R_{Ns} and H_G were all positive, and H_s was close to zero. In contrast, R_{NL} was negative, indicating surface cooling by longwave radiation. When the eclipse began at 0119 LT, R_{Ns} began to decrease, reaching zero during the total solar eclipse. In contrast, H_G and H_S increased, indicating that heat was supplied to the snow surface from snow deeper than 0.05 m and from the atmosphere, respectively. This flux damped the snow surface cooling, and R_{NL} decreased by approximately 10 W m^{-2} from 0119 to 0209 LT.

[34] After the total solar eclipse finished at 0210 LT (the actual end of the total eclipse was 0209:31 LT, but the radiation data were recorded at 1-min intervals), R_{Ns} began to increase rapidly, whereas H_G and H_S began to decrease. H_S and H_G became negative after 0227 and 0300 LT, respectively, indicating that after these times, heat was removed from the surface to the atmosphere and to snow deeper than 0.05 m. R_{NL} increased after 0210 LT.

4.4. Regional Effects of the Eclipse on Air and Snow Temperatures

[35] The crosshatched areas in Figures 8a–8c show the estimated effect of the eclipse on global solar radiation, air temperature at 1.5 m height, and snow temperature at 0.05 m depth. The upper boundary of the crosshatched area in Figure 8a was drawn by interpolating global solar radiation data without the effect of the eclipse (0000 to 0118 LT and from 0328 to 0359 LT) using a quadratic equation (correlation coefficient r = 0.999). The total loss of global solar radiation by the eclipse ($\Sigma \Delta R_{S\downarrow}$, crosshatched area in Figure 8) was estimated to be 0.60 MJ m^{-2}, which corresponds to 1.6% of daily global solar radiation (36.63 MJ m^{-2}; average of solar radiation 1 day before and 1 day after the eclipse).

[36] The upper boundary of the crosshatched area in Figure 8b was drawn as follows: we assumed that the air temperature at 1.5 m height in a noneclipse condition changes linearly with time. Thus, the air temperature intersected with measured air temperature at 0122 and 0315 LT; between these times, the measured air temperature was affected by the eclipse, as explained in section 3.2. The total loss of air temperature due to the eclipse ($\Sigma \Delta T_{a(1.5)}$, crosshatched area in Figure 8b) was estimated to be 9.57×10^3 K s. Thus, the regional effects of the eclipse on temperature at 1.5 m height ($\lambda_{Ta(1.5)}$) were calculated as follows:

$$\lambda_{Ta(1.5)} = \sum \Delta T_{a(1.5)} / \sum \Delta R_{S\downarrow} = 0.016 \, \mathrm{K} (\mathrm{W}\,\mathrm{m}^{-2})^{-1}. \quad (12)$$

[37] The upper boundary of the crosshatched area in Figure 8c was drawn as follows: we assumed that the air temperature at 0.05 m depth in a noneclipse condition changes linearly with time from 0130 to 0430 LT as for Figure 8b. Thus, the snow temperature intersected with the measured air temperature at 0130 and 0430 LT; during the interval, the measured snow temperature was affected by the eclipse, as discussed in section 3.2. The total loss of snow
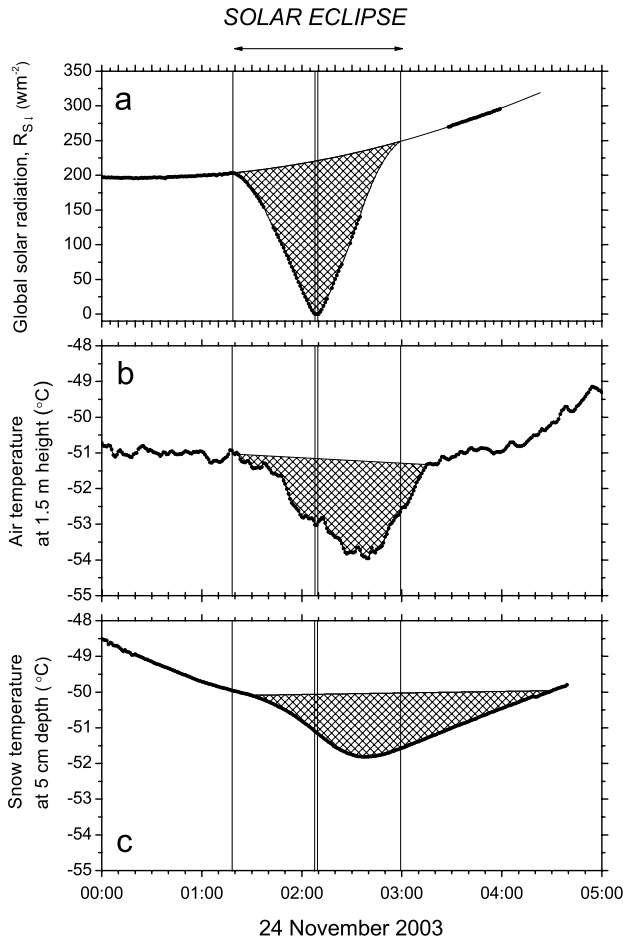
Figure 8. Crosshatched areas show changes in (a) global solar radiation, (b) atmospheric temperature, and (c) snow temperature due to the eclipse. Missing global radiation data were interpolated in Figure 8a. The first, second, third, and fourth contacts are indicated by vertical lines. Local time at Dome Fuji is used (LT = UTC + 3 h).

temperature by the eclipse ($\Sigma \Delta T_{s(0.05)}$, crosshatched area in Figure 8c) was estimated to be 9.98×10^3 K s. Thus, the regional effects of snow temperature at 0.05 m depth ($\lambda_{Ts(0.05)}$) caused by the eclipse were calculated as follows:

$$\lambda_{Ts(0.05)} = \sum \Delta Ts_{(0.05)} / \sum \Delta R_{S\downarrow} = 0.017 \, \text{K} (\text{W m}^{-2})^{-1}. \quad (13)$$

Because of the missing data after 0430 LT (see Figure 8c), this value possibly underestimates the effect of the eclipse on the snow temperature at 0.05 m depth.

[38] The effects of the eclipse on the air temperature at 0.5 m height ($T_{a(0.5)}$) and the surface snow temperature (T_s) are not shown, but were estimated as 0.015 and 0.020 K (W m^{-2})$^{-1}$, respectively. Therefore, the effects of global solar radiation on the atmosphere range from 0.015 to 0.016 K (W m^{-2})$^{-1}$, and the effects on snow range from 0.017 to 0.020 K (W m^{-2})$^{-1}$. If we convert these values to changes for a 1% change in the solar constant (3.4 W m^{-2}; = 1371/4 × 0.01), the ratios for atmospheric air range from 0.051 to 0.069 K and the ratios for snow range from 0.056 to 0.068 K, respectively.

4.5. Relation Between Eclipse Obscuration and Global Solar Radiation

[39] Figure 9a shows the relation between eclipse obscuration (E_O: the fraction of the Sun's surface area occulted by the Moon) and the decreasing ratio of global solar radiation ($R_{S\downarrow}/R_{S\downarrow(1:17)}$) from the first to second contacts. The value of $R_{S\downarrow(1:17)}$ is that of global solar radiation at 0117 LT (203.15 W m^{-2}), which was 1 min before the first contact in 1-min average radiation data. The eclipse magnitude (E_M), the fraction of the Sun's diameter occulted by the Moon, was calculated using "EclipseNaviagator" for the same condition described in section 3.2.1 and was converted to E_O using a simple geometric relation between them. The 1-min average E_O values were calculated using ten E_O values at 6-s intervals, which is identical to the calculation of $R_{S\downarrow}$ described in section 2. The ratio ($R_{S\downarrow}/R_{S\downarrow(1:17)}$) was fitted by the following polynomial equation:

$$R_{S\downarrow}/R_{S\downarrow(1:17)} = 0.4167 E_O{}^3 - 0.6473 E_O{}^2 - 0.7760 E_O + 1.004.$$
$$(14)$$

The correlation coefficient was 0.999. Note that the ratio did not linearly decrease with increasing E_O; two effects, limb darkening of the Sun [e.g., *Ridpath*, 1997] and changes of the vertical solar angle during the eclipse, contribute to this result. A straight line having a slope of −1 is shown by the dotted line in Figure 9a for comparison. We found that
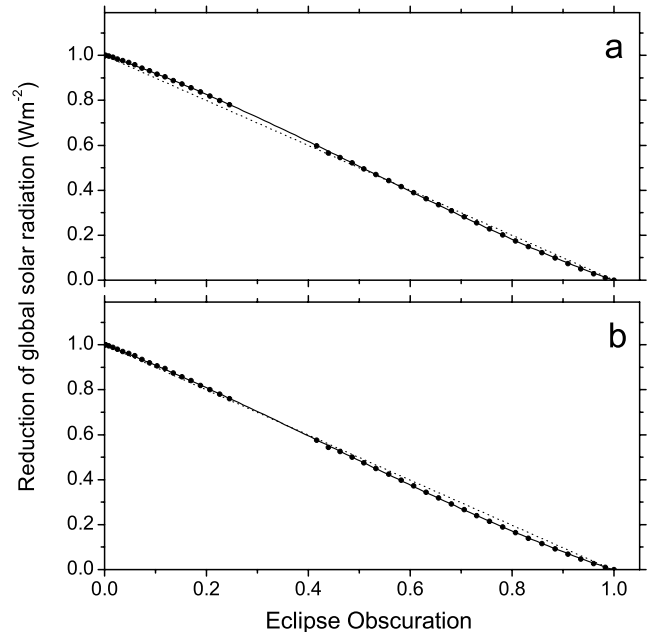

Figure 9. (a) Relation between eclipse obscuration and reduction of global solar radiation ($R_{S\downarrow}/R_{S\downarrow(1:17)}$) from the first to second contacts. The regression line obtained by a polynomial equation is shown by the solid line. (b) Relation between eclipse obscuration and reduction of global solar radiation after correction of solar angle change during the same interval. The regression line obtained by a polynomial equation is shown by the solid line. Straight lines having a slope of −1 are shown with dotted lines in Figures 9a and 9b for comparison.
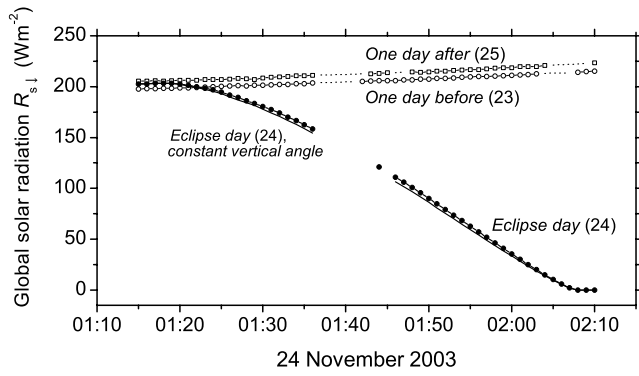
Figure 10. Global solar radiation on 23 (open circles), 24 (solid circles), and 25 (open squares) November 2003 at Dome Fuji. Corrected solar radiation for a constant vertical angle of the Sun on 24 November is shown by a solid line, just below the measured global solar radiation on 24 November. Local time at Dome Fuji is used (LT = UTC + 3 h).

the ratio $R_{S\downarrow}/R_{S\downarrow(1:17)}$ became 0.500 when E_O was 0.505. E_M was 0.579. The maximum difference (0.026) between the ratio and the Sun's surface area $(1 - E_O)$ was observed when E_O was 0.220 at 0135 LT. At the same moment, E_M was 0.332.

[40] Figure 10 shows global solar radiation at Dome Fuji from 0115 to 0210 LT on the day of the eclipse (24 November), and one day before (23) and after (25) the eclipse. Missing data for 23 and 25 November were linearly interpolated and are shown with dotted lines. The weather from 0115 to 0210 LT on these days was quite similar to that on the eclipse day. Thus, we corrected $R_{S\downarrow}$ for the increase in the vertical angle of the Sun $(R*_{S\downarrow})$ as follows:

$$R_{s\downarrow}^* = \frac{R_{s\downarrow}}{R_{s\downarrow(24)}/R_{s\downarrow(1:17)}} \quad (15)$$

$$R_{s\downarrow(24)} = \frac{R_{s\downarrow(23)} + R_{s\downarrow(25)}}{2}. \quad (16)$$

$R_{S\downarrow(24)}$ is estimated global solar radiation without the eclipse using the solar radiation data on 23 and 25 November. The value of $R*_{S\downarrow(24)}$ is shown by the solid line, just below the global solar radiation measured on the eclipse day (24).

[41] Figure 9b shows the relation between the eclipse obscuration and the corrected ratio $(R*_{S\downarrow}/R_{S\downarrow(1:17)})$ expressed as follows:

$$R_{S\downarrow}^*/R_{S\downarrow(1:17)} = R_{S\downarrow}/R_{s\downarrow(24)}$$
$$= 0.3530E_O{}^3 - 0.4701E_O{}^2 - 0.8946E_O + 1.008. \quad (17)$$

The correlation coefficient for the relation was 0.999. For model calculations, global solar radiation during a total solar eclipse can be estimated by equation (17). A straight line having a slope of -1 is also shown by the dotted line in Figure 9b for comparison. Limb darkening of the Sun mainly caused the difference between the two lines in Figure 9b. We found that the corrected ratio became 0.500

when E_O was 0.488, representing a 1.7 percentage point reduction compared to the original $R_{s\downarrow}$ data expressed by equation (14). E_M was 0.581. The maximum difference (0.028) between the ratio $R_{S\downarrow}^*/R_{S\downarrow(1:17)}$ and the Sun's surface area $(1 - E_O)$ was observed when E_O was 0.756 at 0158 LT. At the same moment, E_M was 0.800.

4.6. Comparison to Previous Observations

[42] We summarize the variation in temperature, atmospheric pressure, and wind speed measured during previous total, annular, and partial $(0.90 < E_O)$ eclipses in Table 1. Air temperature from approximately 1.5 to 2.0 m height with clear weather condition decreased from 1.4 to 5.0 K during solar eclipses, with an average of 2.8 K. The time lag from the third contact to the minimum air temperature ranged from 6 to 30 min, with an average of 11.5 min. Thus, the variation in air temperature during the eclipse at Dome Fuji had an average temperature decrease, but a longer time lag, compared to previous studies. The temperature decrease at Dome Fuji was possibly affected by the low thermal emissions from the snow surface at $-54°C$; the longer time lag was possibly caused by the little solar radiation after the eclipse.

[43] We examined the relation among global solar radiation at the first and fourth contacts $(R_{S\downarrow(1st)}$ and $R_{S\downarrow(4th)})$, maximum temperature decrease, and the time lag $(\Delta Time)$ from the third contact in Table 1. We found that the time lag related relatively well to $R_{S\downarrow(4th)}$ for eclipse data collected during a clear weather condition as shown in Figure 11, in which air temperature data measured from 1.5 to 2.0 m above the surface are used. Both types of data have only been recorded at seven sites, namely Kafuka, Japan [*Ueshima et al.*, 1949], Filadelfia, Costa Rica [*Fernández et al.*, 1993a, 1993b], Coronel, Paraguay [*Fernández et al.*, 1996], Springfield, USA [*Segal et al.*, 1996], Kastelorizo, Greece [*Founda et al.*, 2007], Manavgat, Turkey [*Uddin et al.*, 2007], and Dome Fuji. The regression is as follows:

$$\Delta Time = -0.0323 R_{S\downarrow(4th)} + 34.4. \quad (18)$$

In the above equation, the unit of $\Delta Time$ is min, and the correlation coefficient (r) is 0.86. The level of significance for the relation is 0.025 according to a verification of r using Student's t-test $(t = |r|\sqrt{\frac{n-2}{1-r^2}} = 3.794 > t_{0.025} = 3.495$ [*Snedecor and Cochran*, 1968]). The time lag is likely determined by numerous factors such as surface conditions, wind speed, vertical convection rate, and global solar radiation after the eclipse. This result indicates that the global solar radiation after the eclipse $(R_{S\downarrow(4th)})$ mostly determines the period of the time lag. There were no significant relations among the parameters.

[44] *Anderson et al.* [1972] reported that the amplitude of oscillations in atmospheric pressure in nine early measurements from 1887 to 1952, as well as in their own measurements, ranged from 0.1 to 0.45 hPa. *Chimonas* [1973] proposed that Lamb waves were triggered by water vapor cooling in the troposphere. Although the maximum resolution of our atmospheric pressure data was 0.1 hPa, our data show no clear effects of the eclipse on atmospheric pressure. A strong inversion layer (approximately $10-15$ K/300 m) from the surface to approximately 300 m caused by strong radiative cooling at the ice sheet surface [*Hirasawa et al.*,

Table 1. Changes in Temperature, Atmospheric Pressure, and Wind Speed During Total and Annular Eclipses and Partial Eclipses[a]

Date of Eclipse (Maximum Obscuration Percentage)	Location	Weather Condition	Solar Radiation at First and Fourth Contacts (W m−2)	Maximum Temperature Decrease (°C)	Time Lag From the Third Contact[b] (min)	Measurement Height for Temperature (m)	Maximum Change in Atmospheric Pressure (hPa)	Maximum Change in Wind Speed (m s−1)	Reference
1 Jan 1889 (100%)	Willows, Calif., USA	overcast to fair (cloudiness: 6/10 to 2/10, Ci)	nr	3.3	10	1.1	nd	−5.1	Upton and Rotch [1893]
	Red Bluff, Calif., USA	nr	nr	2.8	nr	nr	nd	−2.3	Upton and Rotch [1893]
	Sacrament, Calif., USA	nr	nr	1.7	nr	nr	nd	−2.2	Upton and Rotch [1893]
	Winnemucca, Nebr., USA	nr	nr	1.1	nr	nr	nd	−2.7	Upton and Rotch [1893]
28 May 1900 (100%)	Washington, Ga., USA	clear	nr	2.8	19	nr	~ −0.14	−1.1?	Clayton [1901]
	Wadesboro, N. C., USA	clear	nr	5.0	13	nr	nr	−0.5?	Clayton [1901]
	Virginia beach, Va., USA	nr	nr	4.8	6	nr	nr	nr	Clayton [1901]
8 June 1918 (100%)	Goldendale, Wash., USA	broken to overcast (cloudiness: 8/10), clear at total phase	~1180, ~1150	3.2	10 to 15	nr	−0.19	nr	Kimball and Fergusson [1919]
9 May 1948 (99.9%, annular)	Kafuka, Hokkaido, Japan	clear	960, 940	1.4	8	1.5	nr	nr	Ueshima et al. [1949]
7 Mar 1970 (100%)	Lee, Fla., USA	overcast; sun not visible	nr	3.2	≃0 ("just after")	0.3	0.25	nr	Anderson et al. [1972]
10 July 1972 (90%, partial)	West Penn Island, Canada	clear to cloudy	~750, nr	10	≃0	nr	nr	nr	Stewart and Rouse [1974]
30 June 1973 (100%)	Chinguetti, Mauritania	nr	nr	3.5 / 2.5 / 2.5	10 / 14 / 14	0.3 / 6.75 / 13.5	nd	−4.5	Anderson and Keefer [1975]
26 Feb 1979 (100%)	Hecla Island, Manitoba, Canada	overcast, thin broken Ci	nr	2.0	9	1.5	nr	nd	Anderson [1999]
11 July 1991 (100%)	Filadelfia, Costa Rica	cloudy to clear[c]	nr, ~650	~2.0	~11	~1.5[c]	nr	−4.0	Fernández et al. [1993a, 1993b]
	Santa Cruz, Costa Rica	clear to partly cloudy[c]	~1050, nr	~2.4	~18	~1.5[c]	nr	−2.7	Fernández et al. [1993a, 1993b]
	Puntarenas, Costa Rica	clear to partly cloudy[c]	~1000, nr	~2.6	~11	~1.5[c]	nr	+2.0[d]	Fernández et al. [1993a, 1993b]
10 May 1994 (89%, annular)	Springfield, Ill., USA	clear; no cloud	~800, ~950	5.0	~7	1.6	nr	nr	Segal et al. [1996]
10 May 1994 (94%, annular)	White Sands, N. M., USA	clear	~460, ~710	5.5 / 0.4	7 / 7	0 / 20	nr	nr	Eaton et al. [1997]
10 May 1994 (annular)	Nowata, Okla., USA	clear to partly cloudy	nr	3.0	16	1.5	nr	nr	Crawford et al. (presented paper, 1995)
3 Nov 1994 (100%)	Coronel Oviedo, Paraguay	clear; no cloud	460, 720	3.3	6	1.5	nd[e]	−1.6	Fernández et al. [1996]

Table 1. (continued)

Date of Eclipse (Maximum Obscuration Percentage)	Location	Weather Condition	Solar Radiation at First and Fourth Contacts (W m^{-2})	Maximum Temperature Decrease (°C)	Time Lag From the Third Contact[b] (min)	Measurement Height for Temperature (m)	Maximum Change in Atmospheric Pressure (hPa)	Maximum Change in Wind Speed (m s^{-1})	Reference
11 Aug 1999 (100%)	Freising-Weihenstephan, Germany	overcast (thin cloud)	1070, 1135	1.5 ~2.0 0.2 nd	19 ~11 34	6.0 0 −0.02[g] −0.05 to −0.2[g]	nr	−2.0[f]	*Foken et al.* [2001]
	Fülöpháza, Hungary	clear (cloudiness: 1/8)	nr	~2.5	nr	nr	nr	nr	*Foken et al.* [2001]
	Plittersdorf Met Station, Germany	overcast	500, 500	1.7 to 2.1	4	2	nr	−1.9 at 17 m	*Ahrens et al.* [2001]
11 Aug 1999 (97%, partial)	Reading, UK	clear to partly cloudy	~600, ~800	~3.0	14	1	0.1	~1.0	*Aplin and Harrison* [2003]
23 Nov 2003 (100%)	Dome Fuji, East Antarctica	clear; no cloud	203, 269	3.0 3.3 4.6[h] 1.8	30 20 0 30	1.5 0.5 0 −0.05[i]	nd	−0.3?	this study
29 Mar 2006 (100%)	Kastelorizo, Greece	clear to partly cloudy	894, 734	2.3	12	2.0	−1.8	4.0 to 5.0[d] (approx. −1.0)[j]	*Founda et al.* [2007]
	Manavgat, Antalya, Turkey	clear to partly cloudy	~850, ~700	2.5	6	~1.5	nr	nr	*Uddin et al.* [2007]

[a] Abbreviations: nr, not reported; nd, not detected. Eclipse obscuration: $0.90 < E_O$.
[b] For total solar eclipse, maximum eclipse for annular and partial eclipses.
[c] W. Fernández, personal communication, 2009.
[d] Effect of the eclipse is doubtful.
[e] Sensor resolution is 1 hPa.
[f] Thirty minutes after the minimum of $R_{s\downarrow}$.
[g] In soil.
[h] Estimated.
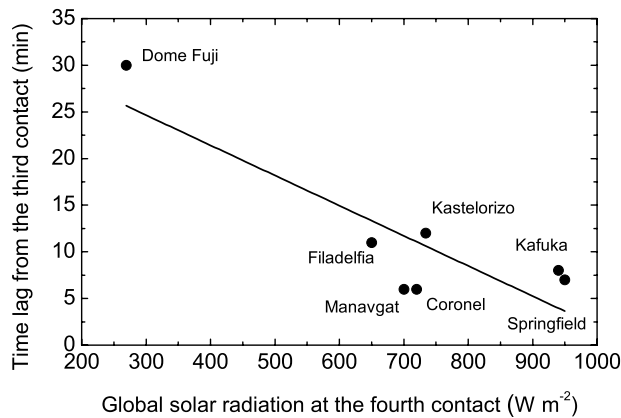[i] In snow.
[j] At Finokalia (95.6% obscuration).

Figure 11. Relation of the global solar radiation at the fourth contact and the time lag of the minimum air temperature at 1.5–1.6 m height to the minimum global solar radiation caused by the eclipse. Only observations made during fine weather are shown. Table 1 provides data measured at Kafuka (Japan), Filadelfia (Costa Rica), Coronel (Paraguay), Springfield (United States), Kastelorizo (Greece), Manavgat (Turkey), and Dome Fuji (East Antarctica).

1999] may have affected the original effects of the eclipse. We should consider this possibility in detail in model calculations [e.g., *Eckermann et al.*, 2007].

[45] Some previous eclipse observations showed that wind speed decreased with decreasing air temperature [e.g., *Anderson and Keefer*, 1975; *Fernández et al.*, 1996; *Ahrens et al.*, 2001; *Aplin and Harrison*, 2003]. Logically, the gradual cooling of the boundary layer and the reduction in turbulent transport as the atmosphere stabilizes should reduce the wind speed during a solar eclipse [*Anderson*, 1999; *Ahrens et al.*, 2001]. At Dome Fuji, wind speed decreased at 0.3 m/s with decreasing air temperature from 0220 to 0248 LT. However, natural variations in wind speed before and after the eclipse made it difficult to identify a "true effect" of the solar eclipse on wind speed.

5. Conclusions

[46] We have investigated the meteorological characteristics during a total solar eclipse at Dome Fuji. The air temperatures at 1.5 and 0.5 m from the snow surface decreased by 3.0 and 3.3 K, respectively, owing to the solar eclipse. Subsurface (0.05 m depth in snow) and estimated surface-snow temperatures decreased by 1.8 and 4.6 K, respectively. Atmospheric pressure did not change owing to the solar eclipse. Wind speed showed a decrease of 0.3 m/s as air temperature decreased. However, natural variations in wind speed before and after the eclipse made it difficult to determine whether the solar eclipse had an actual effect on wind speed. There was no clear effect on wind direction during the solar eclipse. The effect of thermal inertia of sensors for rapidly changing parameters (global solar radiation, reflected solar radiation, air temperatures, and snow temperatures) was examined.

[47] Variations of energy components (net shortwave and longwave radiations, sensible and latent heat fluxes, and geothermal heat) during the eclipse were also examined, although there was an unexplained residual term (average 6.0 W m^{-2}) in the energy budget calculations. The total loss of global solar radiation during the solar eclipse was 0.60 MJ m^{-2}, which corresponds to 1.6% of the total global solar radiation for a day without an eclipse. The sensitivity of air temperatures at 1.5 and 0.5 m height due to changes in global solar radiation ranged from 0.015 to 0.016 K (W m^{-2})$^{-1}$, whereas that of snow temperatures at 0.05 m depth and the surface ranged from 0.017 to 0.020 K (W m^{-2})$^{-1}$.

[48] The comparison to previous observational results from annular and total solar eclipses indicated that the maximum decrease in air temperature during the solar eclipse at Dome Fuji (−3.0 K and −3.3 K at 1.5 m and 0.5 m heights, respectively, from the snow surface) was average, but the time lag was long. Using eclipse data from Kafuka (Japan), Filadelfia (Costa Rica), Coronel (Paraguay), Springfield (USA), Kastelorizo (Greece), Manavgat (Turkey), and Dome Fuji (East Antarctica), we found that the global solar radiation at the fourth contact was linearly related to the period of the time lag. This indicates that the global solar radiation after the eclipse mostly determined the period of the time lag. The relation between eclipse obscuration (E_O, the fraction of the Sun's surface area occulted by the Moon) and the decreasing ratio of global solar radiation from the first to second contacts was also examined. The results showed that the ratio did not linearly decrease with increasing E_O, which was mainly caused by limb darkening of the Sun.

[49] The observational results of this study will contribute to detailed model calculations to clarify the meteorological effects of eclipses on the atmosphere [e.g., *Eckermann et al.*, 2007], especially for eclipses over the Antarctic ice sheet. Observations during the next total solar eclipse over the West Antarctic ice sheet on 4 December 2021 [*Espenak and Meeus*, 2006] can be used to verify our observational results and model calculations.

Appendix A

[50] Since Captain James Cook first sailed around Antarctica in the 1770s, 18 total solar eclipses occurred over Antarctica [*Espenak and Meeus*, 2006]. Table A1 summarizes these eclipses. Although Antarctic explorers since the 1770s might have observed a total solar eclipse over Antarctica, we cannot find any descriptions in their reports.

[51] Since the International Geophysical Year in 1957–1958, three total solar eclipses occurred over Antarctica: 23 October 1957, 12 November 1985, and 23 November 2003. The total solar eclipse on 23 October 1957 occurred about 65 km northwest from Halley Base. D. L. M. Cansfield (Eclipse Oct 23rd 1957: Note on ionospheric soundings, in Ionospheric report for Halley Bay 1957, unpublished report for the British Antarctic Survey, 1958) briefly described a result of vertical ionospheric soundings made during the partial eclipse at Halley Base. Members of Royal Society International Geophysical Year Expedition II stayed at the base. According to the British Antarctic Survey Archive Service, however, probably no one at the Halley Base observed the total solar eclipse.

[52] The total solar eclipse on 12 November 1985 occurred over former Hallett Station, which was built in

Table A1. Total Solar Eclipses Over Antarctica Since 1770

Number	Date	Saros Series	Observation Area[a]
1	20 Feb 1784	117	Victoria Land
2	4 Mar 1802	117	Enderby Land, Dronning Maud Land
3	9 Oct 1809	121	East Dronning Maud Land, Enderby Land, Mac Robertson Land, American High Land
4	14 Mar 1820	117	Palmer Land, Ellesworth Land
5[b]	20 Oct 1827	121	Antarctic Peninsula, Dronning Maud Land, East Dronning Maud Land
6	25 Mar 1838	117	Victoria Land
7[b]	30 Oct 1845	121	Wilkes Land, Victoria Land
8	5 Apr 1856	117	American High Land, East Dronning Maud Land
9	16 Apr 1874	117	Ronne Ice shelf, Berkner Island
10	8 Sep 1885	123	Ellesworth Land
11	26 Apr 1892	117	Marrie Byrd Land
12	21 Sep 1903	123	Wilkes Land
13	9 May 1910	117	Wilkes Land
14	1 Oct 1921	123	Antarctic Peninsula, Filchner Ice Shelf, South Pole
15	12 Oct 1939	123	Wilkes Land, Victoria Land, Dome A region
16	23 Oct 1957	123	Coats Land (ca. 65 km NW from Halley)
17	12 Nov 1985	152	Victoria Land (Hallett)
18	23 Nov 2003	152	Wilkes Land (Mirnyy), Dome Fuji region (Dome Fuji), Dronning Maud Land (Novolazarevskaya, Maitri)
19	4 Dec 2021	152	Ronne Ice Shelf (Filchner), Marie Byrd Land (Byrd)
20	14 Dec 2039	152	Ross Ice Shelf (Scot, McMurdo), Dome A region, Amery Ice Shelf (Davis, Zhong Shan)

[a]Research stations in the area are expressed in parentheses.
[b]Hybrid eclipse; this is also known as an annular total eclipse.

February 1957 in Victoria Land by joint efforts of the United States and New Zealand; this station was active until 1973. *Graham* [1985a, 1985b] introduced the eclipse for the encouragement of observations; however, probably no persons observed that total solar eclipse. Antarctica New Zealand also verifies that no persons stayed at Hallett Station for observations. Thus, we consider that the total solar eclipse on 23 November 2003 was the first total solar eclipse that was observed in Antarctica.

References

Ahrens, D., M. G. Iziomon, L. Jaeger, A. Matzarakis, and H. Mayer (2001), Impacts of the solar eclipse of 11 August 1999 on routinely recorded meteorological and air quality data in south-west Germany, *Meteorol. Z.*, *10*, 215–223, doi:10.1127/0941-2948/2001/0010-0215.

Albrecht, B., M. Poellot, and S. K. Cox (1974), Pyrgeometer measurement from aircraft, *Rev. Sci. Instrum.*, *45*, 33–38, doi:10.1063/1.1686443.

Anderson, J. (1999), Meteorological changes during a solar eclipse, *Weather*, *54*, 207–215.

Anderson, R. C., and D. R. Keefer (1975), Observation of the temperature and pressure changes during the 30 June 1973 solar eclipse, *J. Atmos. Sci.*, *32*, 228–231, doi:10.1175/1520-0469(1975)032<0228:OOTTAP>2.0.CO;2.

Anderson, R. C., D. R. Keefer, and O. E. Myers (1972), Atmospheric pressure and temperature changes during the 7 March 1970 solar eclipse, *J. Atmos. Sci.*, *29*, 583–587, doi:10.1175/1520-0469(1972)029<0583:APATCD>2.0.CO;2.

Aplin, K. L., and R. G. Harrison (2003), Meteorological effects of the eclipse of 11 August 1999 in cloudy and clear conditions, *Proc. R. Soc. A*, *459*, 353–371, doi:10.1098/rspa.2002.1042.

Arya, S. P. (2001), *Introduction to Micrometeorology*, *Int. Geophys. Ser.*, vol. 79, 2nd ed., edited by R. Dmowska, J. R. Holton, and H. T. Rossby, Academic, San Diego, Calif.

Brock, F. V., and S. J. Richardson (2001), *Meteorological measurement systems*, 290 pp., Oxford Univ. Press, Oxford.

Chimonas, G. (1973), Lamb waves generated by the 1970 solar eclipse, *Planet. Space Sci.*, *21*, 1843–1854, doi:10.1016/0032-0633(73)90115-3.

Clayton, H. H. (1901), *The Eclipse Cyclone and the Diurnal Cyclones*, *Ann. Astron. Obs. Harvard College*, vol. 43, part 1, pp. 5–33, Harvard Obs., Cambridge, Mass.

Eaton, F. D., J. R. Hines, W. H. Hatch, R. M. Cionco, J. Byers, D. Garvey, and D. R. Miller (1997), Solar eclipse effects observed in the planetary boundary layer over desert, *Boundary Layer Meteorol.*, *83*, 331–346, doi:10.1023/A:1000219210055.

Eckermann, S. D., D. Broutman, M. T. Stollberg, J. Ma, J. P. McCormack, and T. F. Hogan (2007), Atmospheric effects of the total solar eclipse of 4 December 2002 simulated with a high-altitude global model, *J. Geophys. Res.*, *112*, D14105, doi:10.1029/2006JD007880.

Esaki, Y., O. Sugita, K. Torii, T. Takahashi, and M. Adachi (2007), Meteorological observations at Syowa Station and Dome Fuji Station in 2003 by the 44th Japanese Antarctic Research Expedition (in Japanese with English abstract), *Nankyoku Shiryo*, *51*(2), 129–208.

Espenak, F., and J. Anderson (2002), Annular and total solar eclipses of 2003, *NASA Tech. Pap., 2002–211618*, 75 pp.

Espenak, F., and J. Meeus (2006), Five Millennium Canon of Solar Eclipses: −1999 to +3000 (2000 BCE to 3000 CE), *NASA Tech. Pap., 2006–214141*, 648 pp.

Fernández, W., V. Castro, J. Wright, H. Hidalgo, and A. Sáenz (1993a), Changes in solar irradiance and atmospheric turbidity in Costa Rica

during the total solar eclipse of July 11, 1991, *Earth Moon Planets*, *63*, 119–132, doi:10.1007/BF00575101.

Fernández, W., V. Castro, and H. Hidalgo (1993b), Air temperature and wind changes in Costa Rica during the total solar eclipse of July 11, 1991, *Earth Moon Planets*, *63*, 133–147, doi:10.1007/BF00575102.

Fernández, W., H. Hidalgo, G. Coronel, and E. Morales (1996), Changes in meteorological variables in Coronel Oviedo, Paraguay, during the total solar eclipse of 3 November 1994, *Earth Moon Planets*, *74*, 49–59, doi:10.1007/BF00118721.

Foken, T. (2008), *Micrometeorology*, 306 pp., Springer, Berlin.

Foken, T., B. Wichura, O. Klemm, J. Gerchau, M. Wintherhalter, and T. Weidinger (2001), Micrometeorological measurements during total solar eclipse of August 11, 1999, *Meteorol. Z.*, *10*, 171–178, doi:10.1127/0941-2948/2001/0010-0171.

Founda, D., D. Melas, S. Lykoudis, I. Lisaridis, E. Gerasopoulos, G. Kouvarakis, M. Petrakis, and C. Zerefos (2007), The effect of the total solar eclipse of 29 March 2006 on meteorological variables in Greece, *Atmos. Chem. Phys. Discuss.*, *7*, 10,631–10,667.

Garasopoulos, E. (2007), The total solar eclipse of March 2006: Overview, *Atmos. Chem. Phys. Discuss.*, *7*, 17,663–17,704.

Graham, F. (1985a), Prospects in Antarctica for the total solar eclipse of 12 November 1985, *Polar Rec.*, *22*(141), 681–683.

Graham, F. (1985b), Solar eclipse predicted for Antarctica in November 1985, *Antarct. J. U.S.*, *20*(2), 20–21.

Gross, P., and A. Hense (1999), Effects of a total solar eclipse on the mesoscale atmospheric circulation over Europe—A model experiment, *Meteorol. Atmos. Phys.*, *71*, 229–242, doi:10.1007/s007030050057.

Hanna, E. (2000), Meteorological effects of the solar eclipse of 11 August 1999, *Weather*, *55*, 430–446.

Hirasawa, N., and K. Fujita (2008), Radiation observation at Dome Fuji Station, Antarctica (in Japanese with English abstract), *Nankyoku Shiryo*, *52*, 170–181.

Hirasawa, N., M. Hayashi, S. Kaneto, and T. Yamanouchi (1999), Data report on atmospheric circulation and material cycle in the Antarctic, part 1: Aerological sounding data at Dome Fuji Station in 1997, *JARE DATA Rep. 238*, 183 pp., Nat. Inst. of Polar Res., Tokyo.

Japan Meteorological Agency (2005), *Antarctic meteorological data obtained by the Japanese Antarctic Research Expedition*, vol. 28, *Meteorological Data at Syowa Station and Dome Fuji Station in 2003* [CD-ROM], Tokyo.

Kameda, T., N. Azuma, T. Furukawa, Y. Ageta, and S. Takahashi (1997), Surface mass balance, sublimation and snow temperatures at Dome Fuji Station, Antarctica, in 1995, *Proc. NIPR Symp. Polar Meteorol. Glaciol.*, *11*, 24–34.

Kameda, T., I. Obinata, K. Takahashi, K. Taniguchi, O. Sugita, K. Fujita, K. Kurisaki, and K. Nakano (2005), Construction on a new deep ice coring site at Dome Fuji Station—Operations carried out by the JARE-44 Dome Fuji overwintering team (in Japanese with English abstract), *Nankyoku Shiryo*, *49*, 207–243.

Kameda, T., K. Fujita, O. Sugita, and G. Hashida (2007), Glaciological Data collected by the 44th Japanese Antarctic Research Expedition during 2003–2004, *JARE DATA Rep. 298*, 92 pp., Nat. Inst. of Polar Res., Tokyo.

Kameda, T., H. Motoyama, S. Fujita, and S. Takahashi (2008), Temporal and spatial variability of surface mass balance at Dome Fuji, East Antarctica, by the stake method from 1995 to 2006, *J. Glaciol.*, *54*(184), 107–116, doi:10.3189/002214308784409062.

Kimball, H. H., and S. P. Fergusson (1919), Influence of the solar eclipse of June 8, 1918, upon radiation and other meteorological elements, *Mon. Weather Rev.*, *47*, 5–19, doi:10.1175/1520-0493(1919)47<5:IOTSEO>2.0.CO;2.

King, J. C., and W. M. Connolley (1997), Validation of the surface energy balance over the Antarctic ice sheets in the U.K. Meteorological Office Unified Climate Model, *J. Clim.*, *10*, 1273–1287, doi:10.1175/1520-0442(1997)010<1273:VOTSEB>2.0.CO;2.

Kondo, J. (2000), *Atmospheric Science Near the Ground Surface (in Japanese)*, 324 pp., Univ. of Tokyo Press, Tokyo.

Kondo, J., and H. Yamazawa (1986), Bulk transfer coefficient over snow surface, *Boundary Layer Meteorol.*, *34*, 123–125, doi:10.1007/BF00120912.

Lange, M. A. (1984), Measurements of thermal parameters in Antarctic snow and firn, *Ann. Glaciol.*, *6*, 100–104.

Leeds-Harrison, P., E. G. Youngs, and D. W. K. Blackburn (2000), Soil temperatures during the solar eclipse on 11 August 1999, *Eur. J. Soil Sci.*, *51*, 183–184, doi:10.1046/j.1365-2389.2000.00293.x.

Mellor, M. (1977), Engineering properties of snow, *J. Glaciol.*, *19*(8), 15–66.

National Astronomical Observatory (2008), *Rika Nenpyo (Chronological Scientific Tables)*, vol. 81, 1058 pp., Maruzen, Tokyo.

Prenosil, T. (2000), The influence of the 11 August 1999 total solar eclipse on the weather over central Europe, *Meteorol. Z.*, *9*, 351–359.

Rashid, Z. A. A., M. A. Momani, S. Sulaiman, M. A. M. Ali, B. Yatim, G. Fraser, and N. Sato (2006), GPS ionospheric TEC measurement during the 23rd November 2003 total solar eclipse at Scott Base Antarctica, *J. Atmos. Sol. Terr. Phys.*, *68*, 1219–1236, doi:10.1016/j.jastp.2006.03.006.

Reijmer, C. H., and J. Oerlemans (2002), Temporal and spatial variability of the surface energy balance in Dronning Maud Land, East Antarctica, *J. Geophys. Res.*, *107*(D24), 4759, doi:10.1029/2000JD000110.

Ridpath, I. (1997), *Dictionary of Astronomy*, 536 pp., Oxford Univ. Press, Oxford, U. K.

Royal Aeronautical Society (1972), Characteristics of wind speed in the lower layers of the atmosphere near the ground: Strong winds (neutral atmosphere), *Rep. 72026*, Eng. Sci. Data Unit, London.

Segal, M., R. W. Turner, J. Prusa, R. J. Bitzer, and S. V. Finley (1996), Solar eclipse effect on shelter air temperature, *Bull. Am. Meteorol. Soc.*, *77*, 89–99, doi:10.1175/1520-0477(1996)077<0089:SEEOSA>2.0.CO;2.

Snedecor, G. W., and W. G. Cochran (1968), *Statistical Methods (in English)*, 6th ed., Iowa State Univ. Press, Ames. (Japanese translation by M. Hatamura, C. Okuno, and Z. Tsumura, 546 pp., Iwanami Shoten, Tokyo, 1972.)

Stewart, R. B., and W. R. Rouse (1974), Radiation energy budgets at an Arctic site during the solar eclipse of July 10, 1972, *Arct. Alp. Res.*, *6*(2), 231–236, doi:10.2307/1550088.

Szalowski, K. (2002), The effect of the solar eclipse on the air temperature near the ground, *J. Atmos. Solar Terr. Phys.*, *64*(15), 1589–1600, doi:10.1016/S1364-6826(02)00134-7.

Takahashi, S., and T. Kameda (2007), Snow density for measuring surface mass balance using the stake method, *J. Glaciol.*, *53*(183), 677–680, doi:10.3189/002214307784409360.

Touloukian, Y. S., and T. Makita (1970), *Specific Heat: Nonmetallic Liquids and Gases*, *Thermophys. Prop. Matter*, vol. 6, 300 pp., Plenum, New York.

Uddin, W., B. Joshi, T. S. Kummar, S. Sharma, and R. Sagar (2007), Observations of total solar eclipse of 29 March 2006 and related atmospheric measurements, *Curr. Sci.*, *93*(7), 957–959.

Ueshima, U., F. Narita, Y. Suzuki, and T. Suzuki (1949), The variation of the surface meteorological elements, *Geophys. Mag.*, *19*(3–4), 78–94.

Upton, W., and A. L. Rotch (1893), Meteorological and other observations made at Willows, California, in connection with the total solar eclipse of January 1, 1889, *Annals of the Astronomical Observatory of Harvard College*, vol. 29, part 1, pp. 1–34, Harvard Obs., Cambridge, Mass.

van As, D., M. van den Broeke, C. Reijmer, and R. van de Wal (2005), The summer surface energy balance of the high Antarctic Plateau, *Boundary Layer Meteorol.*, *115*, 289–317, doi:10.1007/s10546-004-4631-1.

Vats, H. O., S. P. Bagare, and S. M. Bhandari (2006), Formation and observations of shadow bands during the total solar eclipse of November 23, 2003 near Maitri, Antarctic, in *Advances in Geosciences*, vol. 2, *Solar Terrestrial*, edited by M. Duldig, pp. 361–368, World Sci., Singapore.

Vogel, B., M. Baldauf, and F. Fiedler (2001), The influence of a solar eclipse on temperature and wind in the Upper-Rhine Valley—A numerical case study, *Meteorol. Z.*, *10*, 207–214, doi:10.1127/0941-2948/2001/0010-0207.

Weller, G., and P. Schwerdtfeger (1977), Thermal properties and heat transfer processes of low-temperature snow, in *Meteorological Studies at Plateau Station, Antarctica*, *Antarct. Res. Ser.*, vol. 25, edited by J. A. Businger, pp. 26–34, AGU, Washington, D. C.

Yamanouchi, T. (1983), Variation of incident solar flux and snow albedo on the solar zenith angle and cloud cover, at Mizuho Station, Antarctica, *J. Meteorol. Soc. Jpn.*, *61*(6), 879–893.

———————————

K. Fujita, Graduate School of Environmental Studies, Nagoya University, Furo-cho, Chikusa-ku, Nagoya 464-8601, Japan.

N. Hirasawa, National Institute of Polar Research, 10-3, Midoricho, Tachikawa, Tokyo 190-8518, Japan.

T. Kameda and S. Takahashi, Snow and Ice Research Laboratory, Kitami Institute of Technology, 165 Koen-cho, Kitami, Hokkaido 090-8507, Japan. (kameda@mail.kitami-it.ac.jp)

O. Sugita, Observations Department, Japan Meteorological Agency, 3-4, Otemachi 1-chome, Chiyoda-ku, Tokyo 100-8122, Japan.